IOPscience iopscience.iop.org

Home Search Collections Journals About Contact us My IOPscience

An x-ray photoemission electron microscope using an electron mirror aberration corrector for the study of complex materials

This article has been downloaded from IOPscience. Please scroll down to see the full text article.

2005 J. Phys.: Condens. Matter 17 S1339

(http://iopscience.iop.org/0953-8984/17/16/005)

View the table of contents for this issue, or go to the journal homepage for more

Download details:
IP Address: 129.252.86.83
The article was downloaded on 27/05/2010 at 20:39

Please note that terms and conditions apply.

INSTITUTE OF PHYSICS PUBLISHING JOURNAL OF PHYSICS: CONDENSED MATTER

J. Phys.: Condens. Matter **17** (2005) S1339–S1350 doi:10.1088/0953-8984/17/16/005

An x-ray photoemission electron microscope using an electron mirror aberration corrector for the study of complex materials

J Feng[1], E Forest[2], A A MacDowell[1], M Marcus[1], H Padmore[1], S Raoux[3], D Robin[1], A Scholl[1], R Schlueter[1], P Schmid[1], J Stöhr[4], W Wan[1], D H Wei[5] and Y Wu[6]

[1] Advanced Light Source, Lawrence Berkeley National Laboratory, Berkeley, CA 94720, USA
[2] High Energy Accelerator Research Organization, 1-1 Oho, Tsukuba, Ibaraki 305-0810, Japan
[3] IBM, Almaden Research Center, 650 Harry Road, San Jose, CA 95120, USA
[4] Stanford Synchrotron Radiation Laboratory, PO Box 20450, Stanford, CA 94309, USA
[5] NSRRC, 101 Hsin-Ann Road, Hsinchu 30077, Taiwan
[6] Department of Physics, Duke University, Durham, NC 27708, USA

Received 9 December 2004, in final form 9 December 2004
Published 8 April 2005
Online at stacks.iop.org/JPhysCM/17/S1339

Abstract

A new ultrahigh-resolution photoemission electron microscope called PEEM3 is being developed at the advanced light source (ALS). An electron mirror combined with a sophisticated magnetic beam separator is used to provide simultaneous correction of spherical and chromatic aberrations. Installed on an elliptically polarized undulator beamline, PEEM3 will be operated with very high spatial resolution and high flux to study the composition, structure, electric and magnetic properties of complex materials.

(Some figures in this article are in colour only in the electronic version)

1. Introduction

The photoemission electron microscope (PEEM) has been developed since 1930 [1, 2] to study the surface and thin film properties of various materials. The x-ray PEEM, which was first built by Tonner [3–5], combines the power of modern synchrotron radiation spectroscopy with the full-field imaging of a PEEM. Different contrast mechanisms such as topographic, elemental, chemical, orientation and magnetic are available with an X-PEEM. In an X-PEEM, x-rays impinging on the sample cause the emission of secondary photoelectrons. These electrons are accelerated to typically 10–30 keV and are focused to produce a magnified intermediate image by an immersion objective lens. Then a series of projection lenses is often used to magnify the intermediate image further and form a final image on a CCD or other imaging detector. The lateral resolution limit of state-of-the-art X-PEEMs such as PEEM2 now operating at the ALS [6] is about 20 nm.

 © 2005 IOP Publishing Ltd Printed in the UK

The resolution of a PEEM, like any electron microscope, is limited by electron diffraction and by spherical and chromatic aberrations of the electron optical system. Electron diffraction can be made sufficiently small by using electrons of high enough energy, and then the system resolution will be limited by residual aberrations. Among these aberrations are astigmatism caused by misalignment and mechanical tolerance which can be compensated by a stigmator, and coma and field distortion are typically insignificant due to a limited imaging area. This leaves chromatic and spherical aberrations as the main factors that limit the resolution. Early in the development of the electron optics theory, Scherzer [7] showed that under the assumption of static field, rotational symmetric lens, a space charge free beam or a beam in which the velocity component does not reverse direction, any lens or lens system always suffers from chromatic and spherical aberrations.

There have been many attempts over the past sixty years or so to search for aberration correction schemes by relinquishing one of the preconditions for the validity of the Scherzer theorem [8]. This is the frontier in electron optics instrumentation development, which would finally allow aberration-free imaging to the atomic scale. By breaking the rotational symmetry, the multipole aberration corrector used by Zach [9, 10] in 1995, based on the theoretical work of Rose [11], produced an improvement in resolution from 6 nm to better than 2.5 nm for a 1 kV scanning electron microscope (SEM). Later, Haider [11–13] improved the resolution in a commercial transmission electron microscope (TEM) from 0.26 to 0.12 nm. Recently, Krivanek [14] achieved a point resolution of 0.123 and 0.076 nm for a 100 and a 120 kV scanning transmission electron microscope (STEM), respectively, using a quadrupole–octupole arrangement. A second possibility for aberration correction is to use time-varying fields [15], which eliminates the static field precondition. Synchrotron radiation sources are ideal for this type of compensation since the source is intrinsically pulsed with lengths typically smaller than 100 ps. An improvement in resolution with a time varying field and pulsed excitation sources has not yet been achieved.

A third class of aberration corrector system is the so-called electron mirror [16–23]. By introducing a reflection in the electron path using an electron mirror, the electron beam direction reverses and the electron velocity changes sign, thus the Scherzer theorem no longer applies. In fact, an electron mirror can have aberration coefficients with opposite signs to those of the lens system, even though it is rotationally symmetric. Therefore the electron mirror can be used to correct the chromatic and spherical aberrations of an electron lens. X-PEEM can benefit greatly from aberration correction since the aberration coefficients of the objective are much larger than those of SEM and TEM objectives due to the wider secondary electron energy distribution and relatively large field of view.

At the ALS, a new x-ray PEEM with a mirror aberration corrector has been designed, and it will be dedicated to the study of complex materials. We refer to this instrument as PEEM3 to indicate that it is the ALS's third-generation PEEM. Another similar project using an electron mirror corrector, SMART (SpectroMicroscope for All Relevant Techniques) in Germany, has been designed as an ultrahigh resolution spectromicroscope for BESSY II [23–27]. Both of these systems are based on the realization of the correction of chromatic and spherical aberration using a type of hyperbolic electron mirror which was pioneered by Rempfer and co-workers [18–20].

2. The PEEM3 concept

The development of PEEM3 is based on the successful design and operation of PEEM2 [6, 28] at the ALS. One of the most exciting research areas with PEEM2 has been the magnetism. The investigation of complex, multi-element magnetic structures [29] has been greatly facilitated

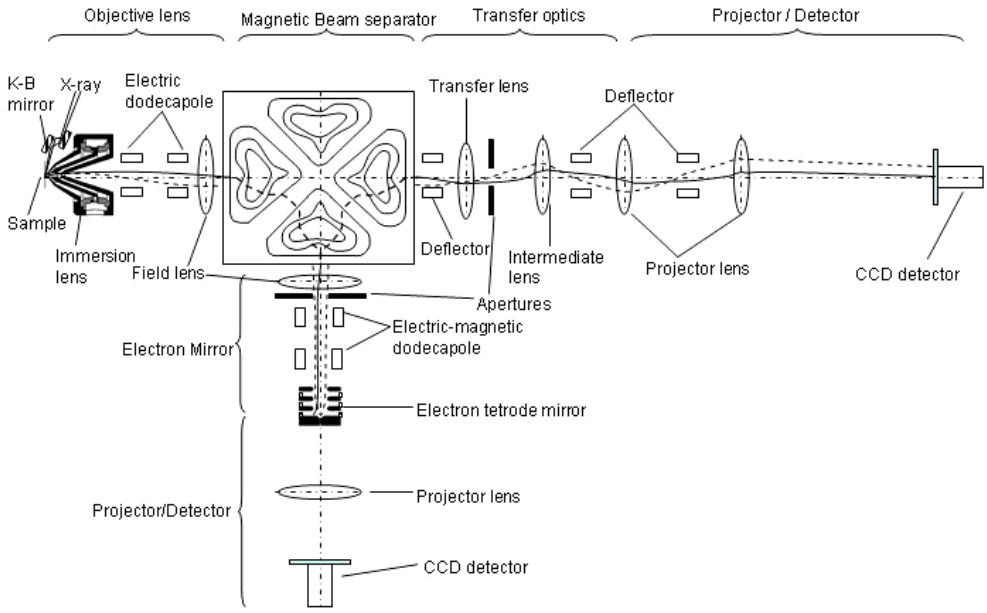

Figure 1. Schematic layout of an x-ray photoemission electron microscope using an electron mirror corrector at the ALS.

by the easy tuning of the x-ray energy and the availability of the linear and circular polarized radiation at modern synchrotron sources combined with the spectromicroscopy technique. A spectacular example of the application of such techniques to problems in interfacial magnetism, in particular the coupling of ultrathin ferromagnetic layers to antiferromagnetic substrates, can be found in [30–32]. The user community requires improvements in sensitivity, spatial resolution, and also the time resolution for the investigation of dynamic process of magnetic system. PEEM3 is designed to have two main operation modes: a high resolution mode and a high flux mode. For the high resolution mode, PEEM3 will achieve a spatial resolution of 5 nm at an efficiency (fraction of emitted electrons arriving at the detector) of a few per cent, which is comparable to that at the best resolution of PEEM2. For the high flux mode, an electron transmission up to 90% is to be realized at a spatial resolution of about 50 nm.

Figure 1 shows the schematic overview of the electron optics of PEEM3. The electrons follow the path shown in dashed lines. The objective lens forms an image plane at the left face of the separator, which subsequently transfers this image plane to the bottom face of the separator. Next the electron beam enters the mirror and then it is reflected back by the mirror, which images with a magnification of -1 at the bottom of the separator. The separator then transfers this new, aberration-corrected image to its right face, where the image is magnified by the transfer, intermediate and projector lenses, finally appearing at the CCD detector. In the objective lens section a set of two electric dodecapoles allows one to ensure that the beam arrives at the separator at the correct position and angle, and also allows stigmation of the image. In the mirror section the two electric–magnetic dodecapoles make it possible to have the electron beam hit the mirror on centre and straight on, and come back to the centre of the bottom face of the separator. The field lens at the left face of the separator causes the field ray to be parallel to the axis, i.e., refers the back focal plane of the objective to a point infinitely far behind the objective. Similarly, the field lens at the bottom of the separator puts an image of the back focal plane of the objective at the effective surface of the mirror. Thus, a ray which

exits the sample slightly above centre but with zero slope (the dotted line in figure 1) arrives below the axis at the separator entrance, comes out of the bottom of the separator to the left of the axis, hits the centre of the mirror, comes back to the bottom of the separator but right of centre, and then is made parallel again by the bottom field lens. After the separator comes a deflector and then a transfer lens, which images the back focal plane onto an aperture of selectable size. Finally the intermediate and projector lenses transfer the image to the CCD with selectable magnification.

The major components briefly sketched above will now be described in more detail.

2.1. X-ray beamline

An elliptically polarized undulator (EPU) at the straight sector 11 of the ALS will be used to produce radiation with continuously variable linear, circular or elliptical polarization. A variable line space (VLS) plane grating monochromator beamline will provide soft x-rays in the spectral range from 100 to 1500 eV. The requirement of absolutely stable energy calibration is of crucial importance for the measurement of small magnetic circular dichroism (MCD) signals, as in most applications of PEEM3. Variable beam sizes on sample from 3 to 50 μm are produced by a pair of bendable Kirkpatrick–Baez mirrors. Additionally, a UV-lamp and a laser system will be mounted to the sample chamber for different purposes such as alignment, commissioning, pump–probe experiment, etc.

2.2. Objective and field lenses

The interaction of photons with a sample generates low energy secondary electrons. These electrons are collected and accelerated by the immersion objective lens to the nominal energy, 20 keV. The objective lens is a pure electrostatic four-electrode lens, in which the sample is also part of the lens and is located at 2 mm away from the second electrode. The distance is changeable to accommodate different sample cases. This objective lens is an asymmetric lens and is similar to the PEEM2 objective lens [6], whose electron optical properties have been optimized to have small aberrations by Rempfer [33] and Watt [34]. An image with a magnification 12 is formed at the entrance plane of the magnetic beam separator. A field lens is located just in front of the entrance of the separator to make the field ray parallel upon entering the beam separator. The objective lens, together with the field lens, forms a telescopic round lens system. This is necessary for the mirror to run in so-called symmetric mode in which first-order chromatic distortion and third-order coma can be cancelled and the curvature of field effect can be reduced [35]. The fundamental ray trajectories through the objective and field lens are shown in figure 2.

2.3. Magnetic beam separator

An electron mirror corrects the spherical and chromatic aberrations of the acceleration field and objective lens. However, practical implementation requires separation of the incoming uncorrected electron beam to the mirror from the corrected outgoing rays to the projector column. A magnetic component can separate inbound and outbound beams. The beam separator consists of four quadrants, each of which acts as a stigmatic 8f transfer system. Thus, the beam is transferred from the left to the bottom face, and from the bottom face to the right, with no change in position or angle. This beam separator itself is not rotationally symmetric, and its dominant aberrations cannot be corrected by the rotationally symmetric mirror. It therefore has to be designed with aberrations below the required resolution of the

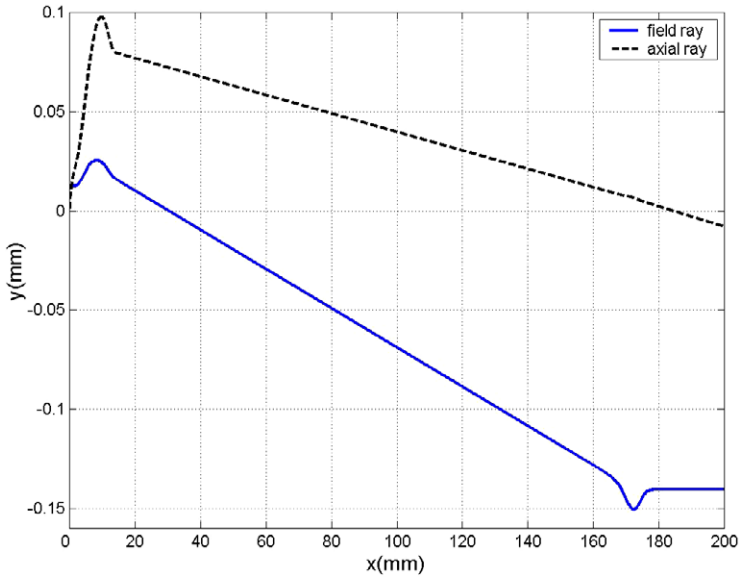

Figure 2. Fundamental ray trajectories of PEEM3 objective lens.

whole microscope. The route to this type separator used in SMART and in PEEM3 was first identified by Rose and Preikszas [35] and further developed in the work of Muller [25].

Like the SMART separator, the PEEM3 separator has a square layout with midsection symmetry and a double mirror symmetry for each quadrant of the magnet. Due to these symmetries, most of the second-order aberrations are cancelled. The imaging property of the beam separator is equivalent to that of a telescopic system of four round lenses. The object side focal plane of the first lens is transferred with unit magnification into the image side focal plane of the fourth lens. During the course of the design process, several separator prototypes with different transverse dimension and vertical gap have been studied using the truncated power series algebra (TPSA) technique [36]. The first trial design had a transverse dimension of 90 cm $\times$ 90 cm and vertical gap of 10 mm. The aberration of this separator exceeds the tolerance. It was then realized that the on-axis aberration of a separator can be reduced by decreasing the size of the magnet. As a compromise of filling factor and model check with SMART, one separator with dimension of 28 cm $\times$ 28 cm and vertical gap of 7 mm was modelled. Detailed information of the design and analysis of the PEEM3 separator can be found in [37]. Accurate calculation of the optical properties of the beam separator largely depends on the assumptions made while developing the field model for the magnet separator. The PEEM3 separator design was done using a localized 2D analytic magnetic field model and checked against finite-element models. When the vertical gap was reduced to 5 mm, the calculated field in the 2D model matches that found by 3D modelling to sufficient accuracy. The specifications and calculated parameters of the separator with 7 and 5 mm gap are given in table 1.

2.4. Electron mirror

The idea of using an electron mirror to correct the chromatic and spherical aberration of a round lens dates back more than half a century [16, 17]. Extensive studies of electron mirrors have been performed by Kelman [38, 39], Rempfer [18–20], Shao [21, 22], and

Table 1. Specifications and calculated parameters of the separator with 7 and 5 mm gap.

Size of magnet (cm)		28	28
Size of gap (mm)		7	5
Width of groove (mm)		3, 6, 3	3, 3, 3
Dispersion at 45°		0	0
Mirror reflection (deg)		22.5, 45	22.5, 45
Total bend angle (deg)		90	90
Current (A)		72.39, −144.78, 72.39	47.68, −95.36, 47.68
Bending electron energy (keV)		20	20
Field (G)		259.6	239.6
Chromatic aberration	X$\alpha\kappa$	−84 mm	−80 mm
	Y$\beta\kappa$	−306 mm	−305 mm
Spherical aberration	X$\alpha\alpha\alpha$	71 mm	64 mm
	X$\alpha\beta\beta$	−362 mm	−355 mm
	Y$\beta\alpha\alpha$	−374 mm	−355 mm
	Y$\beta\beta\beta$	5900 mm	8054 mm

Rose and co-workers [23, 40]. An electron mirror must have a reflecting electrode with a sufficiently negative bias to reverse the axial direction of the electron beam. Since a rotationally symmetric hyperbolic potential distribution can be expressed analytically, both Rempfer [20] and Shao [22] picked up this shape and studied the optical properties of a simple two-electrode hyperbolic mirror. With a simple magnetic separator, Rempfer even demonstrated the principle of correction of spherical and chromatic aberration experimentally by using a two-electrode hyperbolic electron mirror on an electron-optical bench [18].

In 1990, Shao [21] proposed to use an electron mirror which has more than two electrodes and a different shape of the reflecting electrode to adjust the corrected aberration coefficients. Through numerical analysis of a four-electrode electric mirror, Shao showed that spherical and chromatic aberrations can be varied electrically without changing the image distance of the mirror. Later, a more sophisticated theoretical model using a time-dependent perturbation method was developed by Rose [40] and Preikszas [23] to fully understand the mirror system. The integral expressions for the aberration coefficients of a system with large gradients of the trajectories like an electron mirror were derived, and different orders of aberrations of an electron mirror were investigated in detail.

Two very different methods were developed to design the electron mirror for the PEEM3 microscope. The first one uses the industry standard commercial code SIMION [41]. SIMION is an electrostatic and magnetic field modelling program which solves the field using a finite difference method and traces the motion of electron using a fourth-order Range–Kutta integrator. The second one uses the charged-ring method to calculate the field distribution and a differential algebra (DA) technique to track the particle [42]. The DA model approximates the exact solution of the equation of motion with a set of Taylor series of arbitrary but finite order expanded around a certain reference trajectory, and gives Taylor maps. In principle, a DA technique can calculate numerically all aberration coefficients up to arbitrary order. Good agreement has been obtained between these two methods, and a four-electrode mirror has been found to effectively correct the spherical and chromatic aberrations from an objective lens for various operation modes.

Figure 3 shows the effectiveness of the electron mirror in correcting the spherical and chromatic aberrations of an objective lens. To test the spherical aberration, we traced a set of electrons emitted from the sample on-axis, all with the same initial energy 1.33 eV and a range of initial angles (−90° to 90°). The objective lens is tuned for imaging electrons with

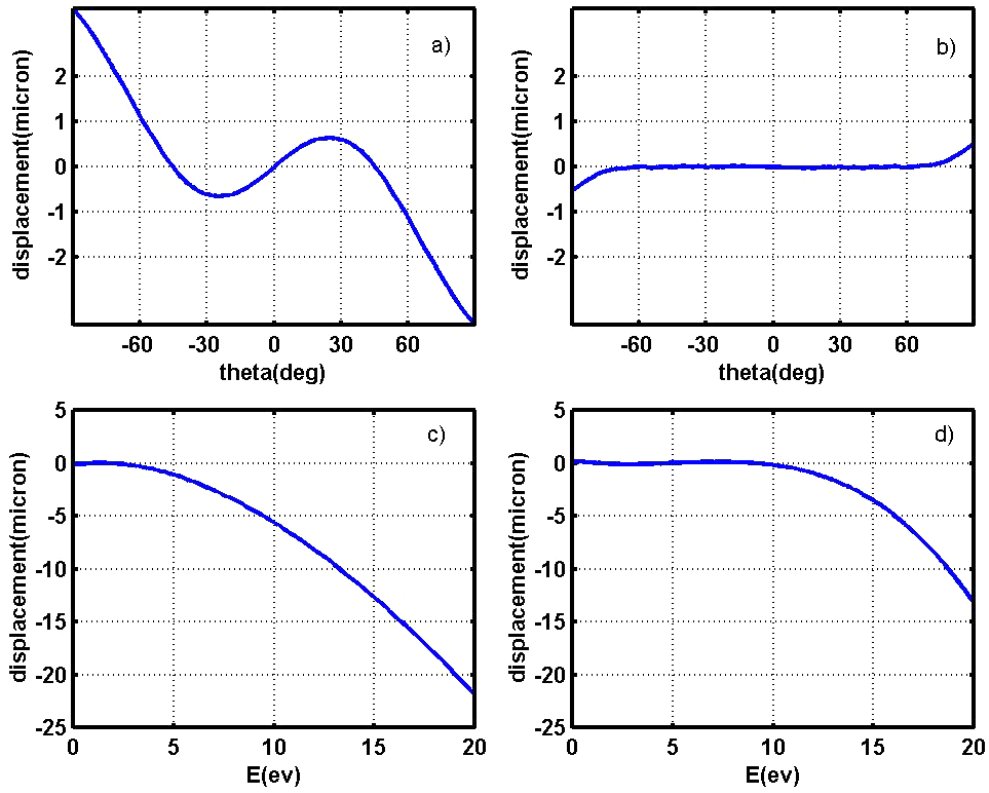

Figure 3. The effectiveness of the electron mirror in correcting the spherical and chromatic aberrations of objective lens. (a) Spherical aberration of objective lens. (b) Spherical aberration corrected by mirror. (c) Chromatic aberration of objective lens. (d) Chromatic aberration corrected by mirror.

an initial angle of 45°. At the image plane of the objective lens, the displacements for each electron are shown in figure 3(a) as a function of initial angle. A straight line along $y = 0$ will be formed if no spherical aberration exists in the objective lens. Due to the spherical aberration of the objective lens, the rays with bigger emitted angle are always more strongly focused than paraxial rays, thus give bigger displacement. Figure 3(b) shows the spherical aberration corrected by the mirror. It clearly shows that electron displacement distribution at the image plane becomes a straight line along $y = 0$ except at the largest angles, where fifth- and higher-order aberrations become important. For the chromatic aberration case, all electrons come off at the same angle but with different initial energies (0–20 eV). Due to the chromatic aberration of the objective lens, slow electrons are always more strongly focused than fast electrons, thus giving a blur at the image plane as shown in figure 3(c). Figure 3(d) presents the effectiveness of the chromatic aberration corrected by the electron mirror, which shows that the faster electrons are focused strongly and the slower electrons weakly, which is a reversal of what the objective lens does and hence gives the chromatic aberration correction.

The PEEM3 electron mirror has four rotationally symmetric electrodes and the reflecting electrode is a segment of a sphere with a radius of 5.6 mm. The inner electrode is put at ground voltage, while the potentials of other electrodes give three free means to determine the focal length, the chromatic aberration and the spherical aberrations of the mirror. In order to cancel

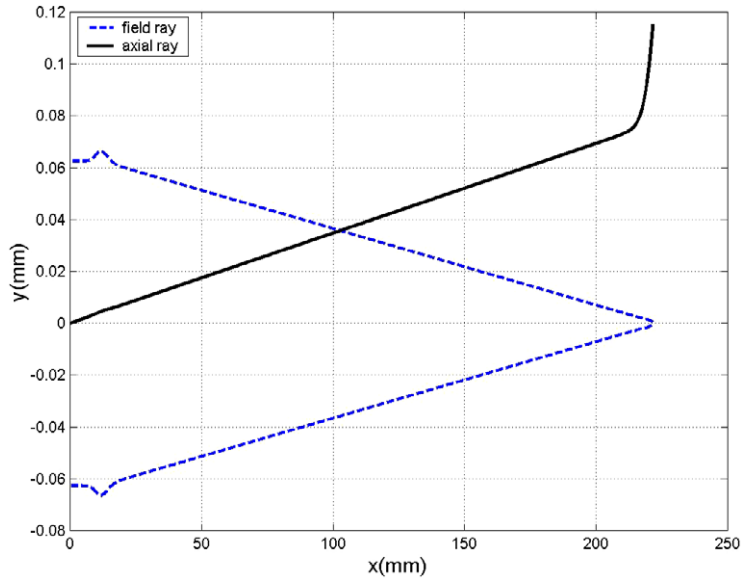

Figure 4. Fundamental ray trajectories of the PEEM3 mirror column.

the coma generated by the mirror, the magnification of the mirror is chosen to be -1, and a field lens is placed near the image plane to ensure that the linear optics is telescopic as shown in figure 4 for the fundamental ray trajectories.

Due to the compact design of the magnetic beam separator, it is difficult to put a beam monitor within the separator. A projector lens and CCD detector are located behind the mirror, which is used as a diagnostic PEEM. This PEEM has similar resolution to PEEM2. It allows us independently to test and optimize the first half of the beam separator and the incoming and outgoing beam at the mirror. In this operation mode, the mirror acts as a unipotential lens and the electron beam passes though a 500 μm diameter hole in the reflecting electrode.

Figure 5 shows the spherical and chromatic aberrations region covered by the PEEM3 mirror. The solid star, rectangle, triangle and circle marks are the aberrations of the objective lens operated in different potential and working distances. The solid curves and dashed curves are the aberrations of the electron mirror with different electrode potential combinations (shown as 0–14 kV for the two middle electrodes of the mirror in the figure) chosen to fix the focal length and adjust the spherical and chromatic aberrations [42]. It shows that our four-electrode mirror covers all the operation modes of the objective lens.

2.5. Transfer optics and projection system

The transfer optics and projection system are used to magnify the intermediate image of the object and source at the exit plane of the magnetic separator onto the CCD detector without distortion. The optical properties of this type of lens with different geometry of individual electrodes have been studied in great detail by Rempfer [43]. Rempfer measured the paraxial optical properties as well as the aberration coefficients of focal length and focal point for a wide range of electrostatic lens geometries. These data are in good agreement with our calculations which are based on SIMION simulation. Therefore, the lenses used in the PEEM3 transfer and projector system are very similar to Rempfer's lenses.

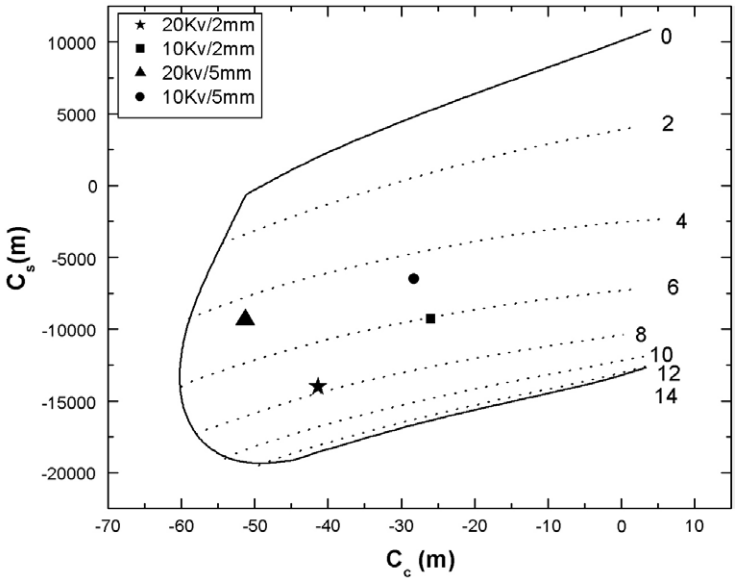

Figure 5. Spherical and chromatic aberration region covered by the PEEM3 electrode mirror and the values required to correct the aberrations of the objective lens for different object potentials and working distances.

After the objective lens has magnified and accelerated the beam, the pencil angle of the electron beam is much reduced from the value θ at the sample to $\sqrt{E/V}\sin\theta/M$, where M is the magnification of the objective lens, E is the emission energy of the electrons from the sample in the range of 0–20 eV, and V is the nominal acceleration voltage of the objective lens (20 kV). Thus all aberrations depending upon angle are very small in the transfer and projection systems due to the small angle entering them. On the other hand, as the beam size at each transfer and projector lens is of the order of a millimetre or greater, the transfer and projector lenses must have distortion aberrations as small as possible. Rempfer [42–44] has proven that a nearly distortionless image can be achieved by two lenses working together when the constraint of having a real object external to the lens is removed. Based on the above consideration, the transfer and projection system of PEEM3 consists of four electrostatic unipotential lenses with the last two lenses being bigger in aperture than the first two. Schematic trajectories of the field ray and axial ray are presented by the dashed curve and solid curve respectively in figure 6. The field ray coming from the magnetic separator exit plane with a zero slope intersects the optics between the first and second lens, where apertures of various diameter are placed. The first transfer lens is operated with a constant potential to give a unit magnification so as to keep the back focal plane image at the aperture. In the high resolution imaging mode, all four lenses are excited. In the high flux imaging mode, the fourth lens can be switched off.

3. Determination of resolution

It is well-known that the resolution of an electron microscope depends not only on the aberrations of electron optics but also on the energy and angular spread of the initial electrons. The secondary electron distribution in x-ray excitation has been studied in detail by Henke [45]. In our model to determine the resolution of PEEM3, the secondary electron distribution

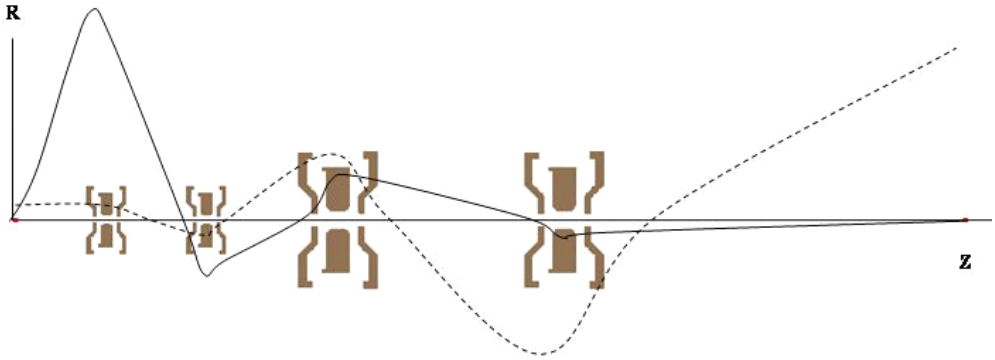

Figure 6. Layout of transfer optics and projection system for the PEEM3 microscope and fundamental ray trajectories.

is represented by a macro-particle model in which each macro-particle carries a weight proportional to the probability density of the initial distribution as given by $E/(E+W)^4\cos(\theta)$. Here, E is the emission energy of the electrons; W is the work function of the sample; θ is the emission angle of the electrons with respect to the sample's normal direction. Then a statistical ensemble of electrons in the sample with initial conditions $E \in (0, 20\ \text{eV})$ and $\theta \in (0, \pi)$ is created. Within our model, we can track the electron beam distribution weighted with the probability anywhere in the system. The resolution is defined as rise-distance of 15%–85% in intensity of the edge scanning the electron point-spread function as used in the SMART project [46].

Diffraction effects arise from the wave nature of electrons, and cause a fundamental limit to the resolving power of an electron microscope, just as the wavelength of light limits the resolution of optical microscopes. In our model, the diffraction effect is calculated for each energy electron and summed up incoherently to yield the point-spread function. Thus the system resolution, referred to the sample, is given by a quadrature addition of resolution from the ray tracing result and diffraction Airy pattern. The comparison of resolution versus transmission for PEEM2 and PEEM3 is shown in figure 7. Operating at 20 kV and 2 mm working distance, the point resolution for 100% transmission reaches 50 nm with the mirror corrector, a significant reduction from that of 440 nm without correction. The best resolution that can be achieved is 5 nm at 2% transmission, as opposed to 20 nm at 1% transmission of PEEM2.

4. Summary

The third-generation PEEM3 at the ALS has been designed. An electron mirror combined with a sophisticated magnetic beam separator is used to provide simultaneous correction of spherical and chromatic aberrations. The PEEM3 electron mirror has four rotationally symmetric electrodes and gives three free means with which to adjust the focal length, the chromatic and the spherical aberrations so that a wide aberration region can be covered for all the operation modes of objective lens. The PEEM3 magnetic separator has a double mirror symmetry configuration which forms a telescopic imaging system with a unit magnification between its entrance and exit planes. The second-order geometrical aberrations and dispersion of first or second degree are cancelled out owing to the intrinsic symmetry at a deflection by 90°. By utilizing polarized radiation from an EPU with a VLS monochromator with high energy

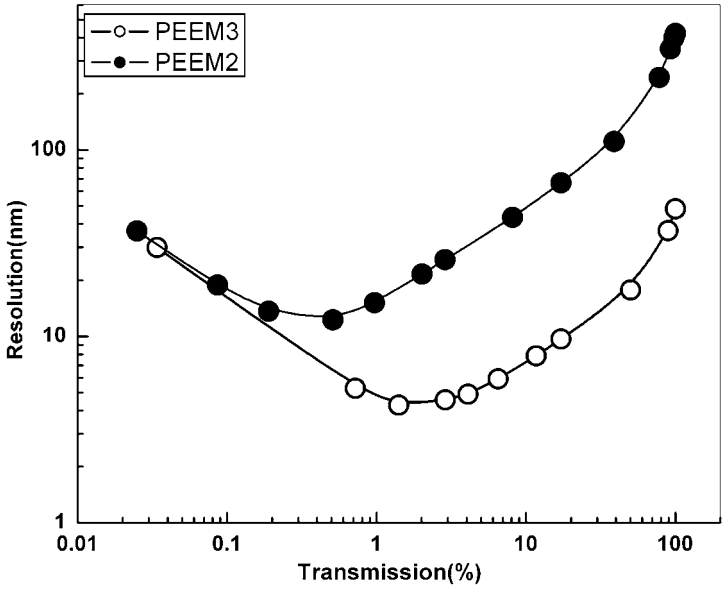

Figure 7. Comparison of resolution versus transmission of PEEM2 and PEEM3. The acceleration potential is 20 kV and the working distance is 2 mm.

stability, PEEM3 allows the study of magnetically ordered systems with high spatial resolution and submonolayer sensitivity. Another significant advantage of the aberration correction is the increase of electron transmission. For a given spatial resolution, comparable with the conventional PEEM, the aperture size of PEEM3 can be made appreciably larger, resulting in a big increase in efficiency over PEEM2. Together with a tighter focusing of x-ray beam, an aberration-corrected X-PEEM such as PEEM3 will allow a significant increase in the image sensitivity and image acquisition speed, which are highly demanded for dynamics studies of complex materials. Therefore, aberration-corrected PEEM will enable spectromicroscopy in whole new dimensions with nanoscale imaging capability [47, 48].

Acknowledgments

We would like to thank M Scheinfein for an early stage of the magnetic separator design, and R Durate, N Kelez, D Munson, K Pertermann, A Doron, H Rose, E Bauer for many helpful discussions.

This work was supported by the Director, Office of Energy Research, Office of Science Of the US Department of Energy, under Contract No. DE-AC03-76SF00098.

References

[1] Brucher E 1933 *Z. Phys.* **86** 448
[2] Griffith O H and Engel W 1991 *Ultramicroscopy* **36** 1
[3] Tonner B, Harp G R, Koranda S F and Zhang J 1992 *Rev. Sci. Instrum.* **63** 564
[4] Tonner B P and Dunham D 1994 *Nucl. Instrum. Methods* A **347** 436
[5] Tonner B P, Dunham D, Dronbacy T, Kikuma J, Denliger J, Rotenberg E and Warwick A 1995 *J. Electron Spectrosc. Relat. Phenom.* **75** 309

[6] Anders S, Padmore H, Duarte R M, Renner T, Stammler T, Scholl A, Scheinfein M, Stohr J, Seve L and Sinkovic B 1999 *Rev. Sci. Instrum.* **70** 3973
[7] Scherzer O 1936 *Z. Phys.* **101** 593
[8] Hawkes P W and Kasper E 1996 *Principles of Electron Optics* vol 2 (New York: Academic) chapter 41
[9] Zach J 1989 *Optik* **83** 30
[10] Zach J and Haider M 1995 *Optik* **98** 112
[11] Rose H 1971 *Optik* **33** 1
[12] Haider M, Rose H, Uhlemann S, Schwan E, Kabius B and Urbam K 1998 *Ultramicroscopy* **75** 53
[13] Haider M, Uhlemann S, Schwan E, Rose H, Kabius B and Urbam K 1998 *Nature* **392** 768
[14] Dellby N, Krivanek O L, Nellist P D, Bateson P E and Lupini A R 2001 *J. Electron Microsc.* **50** 177
Bateson P E, Dellby N and Krivanek O L 2002 *Nature* **428** 617
[15] Schonhense G and Spiecker H 2002 *J. Vac. Sci. Technol.* B **20** 2526
[16] Zworykin V K, Morton G A, Ramberg E G, Hiller J and Vame A W 1945 *Electron Optics and Electron Microscope* (New York: Wiley)
[17] Ramberg E G 1949 *J. Appl. Phys.* **20** 183
[18] Rempfer G F, Desloze D M, Skoczylas W P and Griffith O H 1997 *Microsc. Microanal.* **3** 14
[19] Rempfer G F and Mauck M S 1992 *Optik* **92** 3
[20] Rempfer G F 1990 *J. Appl. Phys.* **67** 6027
[21] Shao Z and Wu X D 1990 *Rev. Sci. Instrum.* **61** 1230
[22] Shao Z and Wu X D 1990 *Optik* **84** 51
[23] Preikszas D and Rose H 1997 *J. Electron Microsc.* **1** 1
[24] Fink R *et al* 1997 *J. Electron Spectrosc. Relat. Phenom.* **84** 231
[25] Muller H, Preikszas D and Rose H 1999 *J. Electron Microsc.* **48** 191
[26] Wichtendahl R *et al* 1998 *Surf. Rev. Lett.* **5** 1249
[27] Schmidt Th *et al* 2002 *Surf. Rev. Lett.* **9** 223
[28] Scholl A, Ohldage H, Nolting F, Stohr J and Padmore H 2002 *Rev. Sci. Instrum.* **73** 1362
[29] Kortright J B, Awschalom D D, Stohr J, Bader S D, Idzerda Y U, Parkin S P, Schuller I K and Siegmann H C 1999 *J. Magn. Magn. Mater.* **207** 2
[30] Ohldag H *et al* 2001 *Phys. Rev. Lett.* **87** 247201
[31] Nolting F, Scholl A, Stohr J, Seo J W, Fompeyrine J, Siegwart H, Locquet J P, Anders S, Luning J, Fullerton E E, Toney M F, Scheinfein M and Padmore H 2000 *Nature* **405** 767
[32] Scholl A, Stohr J, Luning J, Seo J W, Fompeyrine J, Siegwart H, Locquet J P, Nolting F, Anders S, Fullerton E E, Scheinfein M and Padmore H 2000 *Science* **287** 1014
[33] Rempfer G F, Skoczylas W R and Griffin O H 1991 *Ultramicroscopy* **361** 196
[34] Watts R N, Liang S, Levine Z H, Lucatorto T B, Polack F and Scheinfein M 1997 *Rev. Sci. Instrum.* **68** 3464
[35] Rose H and Preikszas D 1992 *Optik* **92** 31
[36] Berz M 1987 *Nucl. Instrum. Methods* A **258** 431
[37] Wu Y K, Robin D S, Forest E, Schlueter R, Anders S, Feng J, Padmore H and Wei D H 2004 *Nucl. Instrum. Methods* A **519** 230
[38] Kelmann V M, Sekunova L M and Yakushev E M 1973 *Sov. Phys.—Tech. Phys.* **17** 2279
Kelmann V M, Sekunova L M and Yakushev E M 1974 *Sov. Phys.—Tech. Phys.* **18** 1142
Kelmann V M, Sekunova L M and Yakushev E M 1974 *Sov. Phys.—Tech. Phys.* **18** 1799
Kelmann V M, Sekunova L M and Yakushev E M 1974 *Sov. Phys.—Tech. Phys.* **18** 1809
[39] Dodic A C and Nesvizkskii M B 1981 *Sov. Phys.—Tech. Phys.* **26** 539
[40] Rose H and Preikszas D 1995 *Nucl. Instrum. Methods* A **363** 301
[41] Dahl D A, Delmore J E and Appelhaus A D 1990 *Rev. Sci. Instrum.* **61** 601
[42] Wan W, Feng J, Padmore H A and Robin D S 2004 *Nucl. Instrum. Methods* A **519** 222
[43] Rempfer G F 1985 *J. Appl. Phys.* **57** 2385
[44] Rempfer G F, Skoczylas W P and Griffith O H 1991 *Ultramicroscopy* **36** 196
[45] Henke B L, Liesegang J and Smith S D 1979 *Phys. Rev.* B **19** 3004
[46] Hartel P, Preiksaz D, Spehr R, Muller H and Rose H 2002 *Advances in Imaging and Electron Physics* vol 120 (Amsterdam: Elsevier Science)
[47] Bauer E 2001 *J. Electron Spetrosc. Relat. Phenom.* **114–116** 975
[48] Bauer E 2001 *J. Phys.: Condens. Matter* **13** 11391